

RESEARCH

Open Access



# Structural and transduction patterns of human-specific polymorphic SVA insertions

Ashley E. Kirby<sup>1,2</sup>, Mark Loftus<sup>1,2</sup>, Emily C. Golba<sup>1</sup>, Human Genome Structural Variation Consortium and Miriam K. Konkel<sup>1,2\*</sup>

## Abstract

**Background** SINE variable number tandem repeat *Alu* elements (SVAs) are a unique group of hominid-specific composite retrotransposons with highly variable internal structure. They represent the youngest TE family in humans and contribute to genetic diversity, evolution, and disease. Recent findings indicate that SVA mobilization rates may exceed previous estimates, and many SVAs exhibit insertion polymorphism. SVAs facilitate transduction (TD) events when transcription initiates upstream of a source element, or when their internal termination signal is bypassed, mobilizing adjacent 5' and/or 3' sequence. To investigate features of non-reference SVA elements currently polymorphic in the human genome, we analyzed a structural variant callset built upon 35 diverse human genomes generated by the Human Genome Structural Variation Consortium.

**Results** In our curated dataset of 543 polymorphic, non-reference SVAs, we identify insertions representing the three youngest subfamilies: D (7%), E (38%), and F (55%). Of the latter, we determine that at least 47% are actually SVA\_F<sub>1</sub>, a more recently discovered human-specific subfamily, indicating that F<sub>1</sub> is a major contributor to SVA expansion in the human population. We further uncover that 40% of non-reference SVAs carry a TD on their 5' and/or 3' ends. Of these, the majority (69%) harbor sequence originating in a gene, including 14 exonic events and the mobilization of a processed pseudogene, supporting the role of SVA in exon shuffling. In addition, we identified a so-called "orphan" TD, defined by the absence of SVA sequence at the insertion site. Leveraging TD origin coordinates, we identify 55 active source elements, including nine non-reference and 46 across GRCh38 and T2T-CHM13, giving rise to 84% of TD-carrying SVAs.

**Conclusions** Our analyses indicate that SVA\_F<sub>1</sub> is more active than previously described and is a main driver of SVA expansion. We find two-fold more TD events compared to previous estimates, with an unexpected bias toward 3' events. Finally, we postulate that the discrepant SVA mobilization rate may be attributed to inter-individual variation in the presence/absence of source elements, a recent uptick in mobilization supported by overall low allele frequencies, and/or negative selection against deleterious insertions.

**Keywords** Retrotransposon, Transposable element, Mobile element insertion, SVA, Subfamily, Polymorphism, Transduction, Source element, Genetic variation, Structural variation, Human specific

## Background

Transposable elements (TEs), mobile units of DNA, are ubiquitous across almost all eukaryotic genomes [1] and are estimated to comprise up to two thirds of the human genome [2–4]. In humans, only three TE families are currently propagating, all of which are non-LTR (long terminal repeat) retrotransposons that mobilize via an

\*Correspondence:

Miriam K. Konkel  
mkonkel@clemson.edu

<sup>1</sup> Department of Genetics and Biochemistry, College of Science, Clemson University, Clemson, South Carolina, USA

<sup>2</sup> Clemson Center for Human Genetics, Clemson University, Greenwood, South Carolina, USA



© The Author(s) 2025. **Open Access** This article is licensed under a Creative Commons Attribution 4.0 International License, which permits use, sharing, adaptation, distribution and reproduction in any medium or format, as long as you give appropriate credit to the original author(s) and the source, provide a link to the Creative Commons licence, and indicate if changes were made. The images or other third party material in this article are included in the article's Creative Commons licence, unless indicated otherwise in a credit line to the material. If material is not included in the article's Creative Commons licence and your intended use is not permitted by statutory regulation or exceeds the permitted use, you will need to obtain permission directly from the copyright holder. To view a copy of this licence, visit <http://creativecommons.org/licenses/by/4.0/>.

RNA intermediate [5–7]. The autonomous L1 (long interspersed element 1) provides the enzymatic machinery for its own integration, as well as for the insertion of the nonautonomous *Alu* and SVA (SINE-variable number tandem repeat-*Alu*) elements [8–10]. Of these, SVA is the evolutionarily youngest TE family, forming in the common ancestor of apes and undergoing expansion in the great apes [7, 11, 12].

SVA elements are unique due to their composite structure, with full-length insertions comprising five distinct units derived from repetitive sequences. Full-length elements are typically 1.5–3 kb in length, though their size is highly variable due primarily to copy number variation in the VNTR and hexameric regions [12]. No internal SVA promoter has been identified, but excision of the hexameric and *Alu* regions in SVA reporter constructs severely attenuates retrotransposition efficiency, suggesting promoter activity in the 5' region [10, 13]. Given the presence of associated features, SVAs are thought to be transcribed by RNA polymerase II and inserted into the genome via L1-mediated target-primed reverse transcription (TPRT) [8–14]. SVA elements exhibit an overall GC composition of ~60%, exceeding 70% in the VNTR [12, 15]. Due to their GC-rich nature, SVAs have been associated with alterations in local chromatin structure and gene expression [16, 17], as well as with the predicted formation of G-quadruplex secondary structures, which have been shown to impact transcription and genome stability [18, 19]. Furthermore, SVAs are associated with altered splice patterns, which may result in differential gene expression [20–22]. Taken together, SVA elements demonstrate immense potential to shape genome structure and function.

In the lineage leading to human, SVAs are commonly divided into six subfamilies (SVA\_A – SVA\_F), with A representing the oldest and F the youngest subfamily [12]. Three parallel studies identified an additional, human-specific subfamily known as SVA\_F<sub>1</sub>, comprised of at least 84 reference (NCBI35/hg17, NCBI36/hg18, and GRCh37/hg19) SVA elements [23–25]. These insertions, characterized by replacement of the hexameric, and the majority of the *Alu*, region with *MAST2* (microtubule associated serine/threonine kinase 2) exon 1 sequence, are likely the result of a non-recurrent ancestral splicing event. [23–25]. Based on whole genome analyses, SVAs are generally thought to be the retrotransposon family with the lowest mobilization rate in the human population, with about 1 new insertion per 916 live births [26]. However, a far higher rate of 1 insertion per 63 births was more recently suggested, based on pedigree analyses [27].

A subset of SVA elements co-mobilize host sequence on their 5' and/or 3' ends, commonly referred to as transductions (TDs), a feature first described for L1 elements

[11, 23–25, 28–33]. While 5' TDs are attributed to upstream promoters and transcription start sites (TSS), 3' TDs result when the internal polyadenylation signal is bypassed in favor of a downstream signal [11, 23–25, 28–31]. Although the overall TD rate estimated for SVA (14–18%) is on par with that described for L1 (10–23%), their 5' and 3' rates differ, with the vast majority of L1-associated TDs being 3' events and SVAs more commonly thought to harbor 5' TDs [11, 23–25, 28–35].

Here, we utilize a non-reference SVA callset built upon 35 individuals to conduct a comprehensive analysis of structural features and elucidate subfamily propagation dynamics within humans. Further, we investigate the prevalence of SVA-mediated TD events and examine the genomic context of transduced sequences. Finally, we utilize TD sequences to identify active source elements driving SVA amplification and examine inter-individual variation in source element abundance.

## Results

### Distribution of non-reference SVA insertions

We first identified 583 putative SVA insertions from the Freeze 4 structural variation (SV) callset, generated by the Human Genome Structural Variation Consortium (HGVC, phase 2) (Table S1), using L1ME-AID (L1-Mediated Annotation and Insertion Detector) (see *Methods*) [36]. For all putative insertions, we retrieved 500 bp of up- and downstream flanking sequence from the assemblies to identify endonuclease cleavage sites and TSDs. We then queried up- and downstream flanking sequences against the human reference genome (GRCh38) using BLAT [37] to confirm the absence of each insertion from the reference. Applying these constraints, we curated a final dataset of 543 high-confidence, non-reference SVA insertions (Table S2).

Next, we investigated the distribution of SVA insertions across chromosomes, which revealed significant deviation from the expected distribution (Chi-square test;  $\chi^2=72.45$ ,  $df=23$ ,  $p<0.01$ ) (Fig. 1a). In particular, we discovered a depletion of insertions on chromosomes 4, X, and Y, and an enrichment on chromosomes 17 and 19 (Fig. 1a). Leveraging the RepeatMasker annotation of GRCh38 [38], we also determined that 55% (297/543) of insertions occurred into TE sequences, with TE class breakdown in alignment with TE background composition in the genome (Table S2; Fig. S1).

Intersection of SVA insertion coordinates with GENCODE information (v46) [39] further revealed that 59% (320/543) (Table S2) of non-reference elements inserted into a gene (protein-coding: 254, 47%; non-coding: 66, 12%). Notably, insertion into protein-coding genes occurred more frequently than expected (Chi-square test;  $\chi^2=7.49$ ,  $df=1$ ,  $p<0.01$ ) based on a

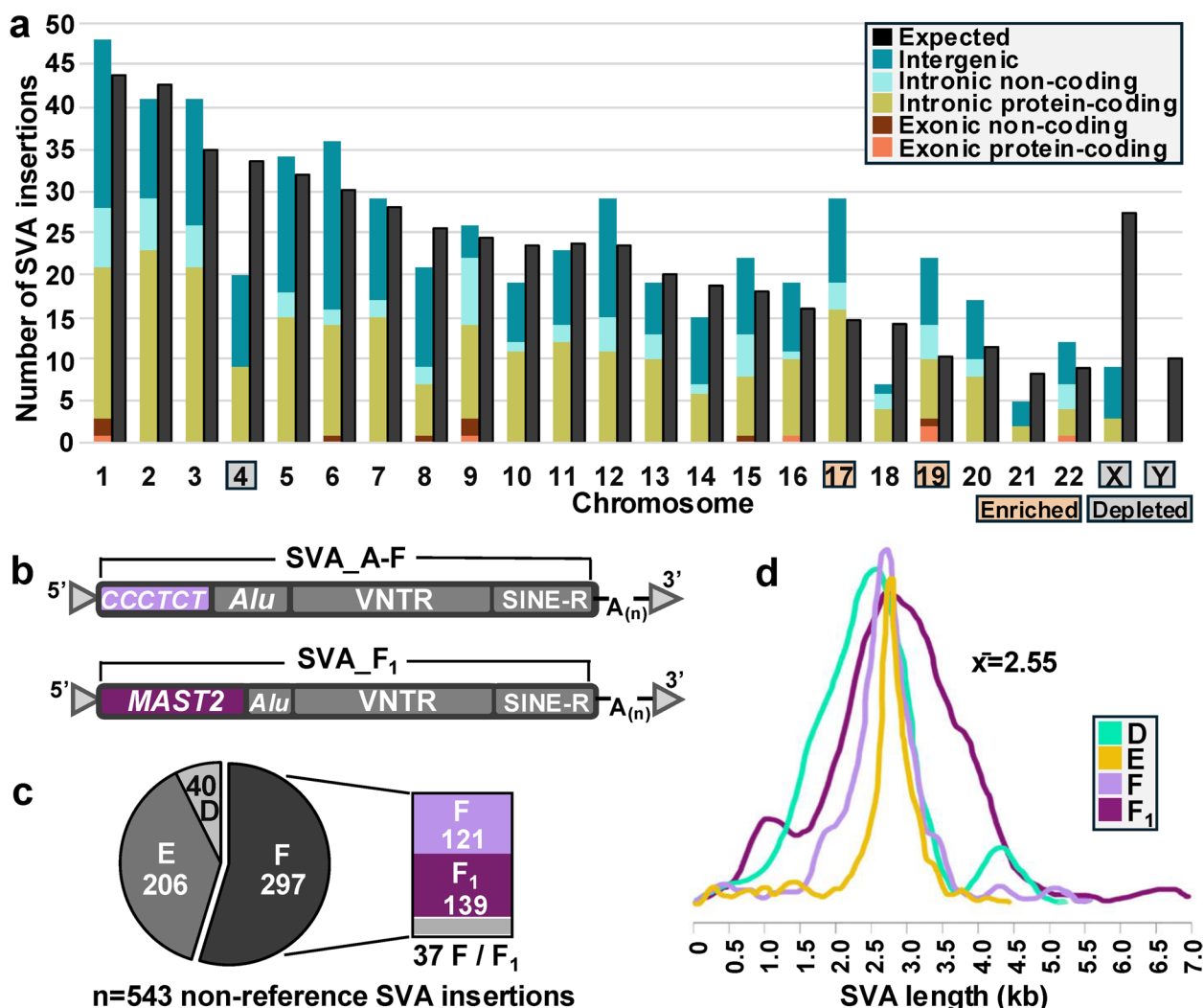


**Fig. 1** SVA element structure and insertion characteristics. **a** Genomic distribution of non-reference SVA elements. The proportion of insertions into intergenic regions, non-protein-coding genes, and protein-coding genes is shown. **b** SVA structures. Top: SVA A-F element. From 5' to 3', these units are commonly described as: (1) a hexameric region, composed of a variable number of CCCTCT repeat units; (2) an *Alu*-like region comprised of two antisense *Alu* fragments; (3) a variable number of tandem repeats (VNTR) region; (4) a short interspersed element of retroviral origin (SINE-R) region derived from the 3' end of the *env* gene and the 3' LTR of the endogenous retrovirus HERV-K10; and (5) a homopolymeric tract of adenosines (i.e., A-tail) [12]. Bottom: An SVA<sub>F1</sub>, where the hexameric region, and most of the *Alu* region, is replaced with *MAST2* exon 1 sequence as the result of an ancestral splicing event from exon 1 of the *MAST2* gene to a cryptic splice site within a polymorphic SVA<sub>F</sub> [24, 25]. **c** Subfamily annotation of non-reference SVAs. Finer-scale resolution of SVA<sub>F</sub> revealed that the majority of insertions are SVA<sub>F1</sub>. **d** Length of non-reference SVA elements by subfamily. Insertions ranged in size from 140 bp to 6.7 kb. By subfamily, SVA<sub>F1</sub> elements were the longest on average (M: 2.88 kb, Mdn: 2.88 kb), followed by SVA<sub>F</sub> (M: 2.56 kb, Mdn: 2.63 kb), SVA<sub>E</sub> (M: 2.55 kb, Mdn: 2.74 kb), and SVA<sub>D</sub> (M: 2.42 kb, Mdn: 2.39 kb)

genomic proportion of 41% (~40% intronic and ~1% exonic) protein-coding sequence [40], further supporting a non-random distribution model. While the majority (306/320) of genic insertions were intronic, we also identified 14 exonic events (6 protein-coding and 8 non-coding), including one insertion into a 5' UTR, 11 into 3' UTRs (including four protein-coding genes *XBPI*, *RPSA2*, *MYCL*, and *PAGRI*), and 2

within protein-coding exons (Table S2). The latter two instances involve an insertion into *SARDH* (sarcosine dehydrogenase), as well as a previously documented insertion into *ZNF404* (zinc finger protein 404) [41]. Given both inserted into the terminal exon, nonsense mediated decay (NMD) would not be triggered, resulting in expression of proteins altered at the carboxy terminus [42, 43].

### SVA characterization

Through alignment of our 543 SVA elements against the SVA\_A-F consensus sequences [44] using MUSCLE (v 3.8.31) [45], we confirmed propagation of the three youngest subfamilies (D-F), with 55% (297/543) identified as SVA\_F, 38% (206/543) as SVA\_E, and 7% (40/543) as SVA\_D (Fig. 1b-c; Table S2). While the younger, human-specific subfamilies E and F drive SVA mobilization, we also identify SVA\_D insertions, which arose prior to the radiation of the human and chimpanzee lineages [12], indicating that they continue to mobilize, albeit at a low rate.

Given that another subfamily, SVA\_F<sub>1</sub>, was previously suggested [23–25], we investigated the abundance of SVA\_F<sub>1</sub> in our dataset. As SVA\_F<sub>1</sub> is regularly not recognized as an independent subfamily, and as the Dfam library used for annotation by RepeatMasker [38] does not include an F<sub>1</sub> consensus sequence [44], we manually screened the subset initially classified as F for the presence of F<sub>1</sub> insertions. Toward this, we performed an MSA against the SVA\_F consensus sequence [45] and manually differentiated F from F<sub>1</sub> (Fig. 1b). Our alignment revealed that F and F<sub>1</sub> insertions are identical downstream from the *MAST2*/SVA splice junction at nucleotide position 385 (Fig. S2). We first identified 230 elements with sequence upstream of this breakpoint, annotating 112 SVA\_F insertions and 118 SVA\_F<sub>1</sub> insertions. Of the remaining 67 elements, which were 5' truncated and initiated within the shared 3' region, we distinguished 9 SVA\_F and 21 SVA\_F<sub>1</sub> elements by leveraging F or F<sub>1</sub>-defining single nucleotide variants (SNVs), indels, and 3' TDs. Only 37 elements remained ambiguous. Thus, finer-scale resolution of the SVA\_F subfamily reveals that SVA\_F<sub>1</sub> generated at least as many, and likely more, insertions based on discernable elements (139 F<sub>1</sub> vs. 121 F) (Fig. 1c).

Further analysis revealed that insertions span an average of 2.6 kb (Mdn: 2.7 kb) (Fig. 1d), and that 60% (325/543) are full length (see *Methods*; Fig. S3). As expected, alignment against SVA consensus sequences uncovered a substantially greater quantity of 5' truncated elements (91%; 199/218) compared to those that were 3' truncated (6%; 12/218) or truncated on both ends (3%; 7/218; confirmed to have proper A-tails) (Fig. S3). Most (90%; 17/19) 3' truncation events clustered around two non-canonical termination sites in the SINE-R region (Fig. 2a; Table S3), which has previously been suggested to contain cryptic polyadenylation signals [12, 33].

The first cluster includes a group of eight SVA\_F elements that terminate 233 bp upstream of the last nucleotide in the canonical polyadenylation signal. All but one share a substitution located 23 bp before the termination point, generating a cryptic polyadenylation signal

((G → A)TTAAA) (Fig. 2a; Table S3). A BLAT query against GRCh38 revealed six additional substitution-carrying 3' truncated SVA\_F elements in the reference genome, providing further evidence for the association of the substitution with recurrent truncation. However, the substitution may not introduce a strong polyadenylation signal, as we also identified eight SVA\_F elements harboring the substitution without 3' truncation. The second cluster of truncated SVAs terminates 323 bp upstream of the canonical signal and contains nine elements across subfamilies D, E, and F<sub>1</sub> (Table S3). Truncation appears to be the result of a weak non-canonical polyadenylation signal (AAGAAA) within the SVA consensus sequence, located 17 bp upstream from the point of termination (Fig. 2a), resulting in recurrent 3' termination across subfamilies. Only one SVA 3' truncated in the SINE-R region terminated outside of the described hotspots.

We also investigated variation within the hexameric and VNTR regions, as well as in poly-A tails. We determined that the hexameric region ranged from 10 to 1068 bp (M: 158 bp, Mdn: 122 bp), with significant length variation across subfamilies D, E, and F (ANOVA;  $F(2, 284)=7.59, p<0.001$ ), and the longest hexamers observed in SVA\_E elements (Fig. 2b). VNTR lengths for all elements (D-F<sub>1</sub>) with a complete VNTR (i.e., not truncated within the region) ranged from 387 to 4150 bp (M: 1740 bp, Mdn: 1696 bp) and also exhibited significant variation (ANOVA;  $F(3,439)=40.79, p<0.001$ ) (Fig. 2c). We noticed an inverse relationship between VNTR size and evolutionary age (i.e., younger elements harbor longer VNTRs), indicating that expansion predominates over contraction and that longer VNTRs are not prohibitive for mobilization. Finally, poly-A tails ranged from 8 to 150 bp (M: 38 bp, Mdn: 35 bp) (Fig. S3). Of note, we found that the majority (70.5%; 383/543) of A-tails contained at least one substitution, while 29.5% of A-tails were uniform.

Our investigation of the hexameric region of non-reference SVA\_D-F elements revealed considerable recurrent deviation from the generally reported (CCCTCT)<sub>n</sub> repeat pattern (Fig. 2d) [11, 12]. To our knowledge, only one such hexameric deviation has been previously noted: a (CCGTCT)<sub>n</sub> repeat, where the “G” was attributed to reverse transcription of the 5' cap and expansion of this addition with the hexamer [20]. Reporting only patterns shared by a minimum of five elements, we identified three hexameric variants and multiple patterns deviating from the classically described hexamer structure, including a 7-mer, 8-mer, 16-mer, 19-mer, and 25-mer (Fig. 2d). We queried GRCh38 and determined that all patterns are also present within reference SVA elements. Furthermore, we found evidence of all but one pattern (GTC TCC) in chimpanzee (panTro6), indicating that these

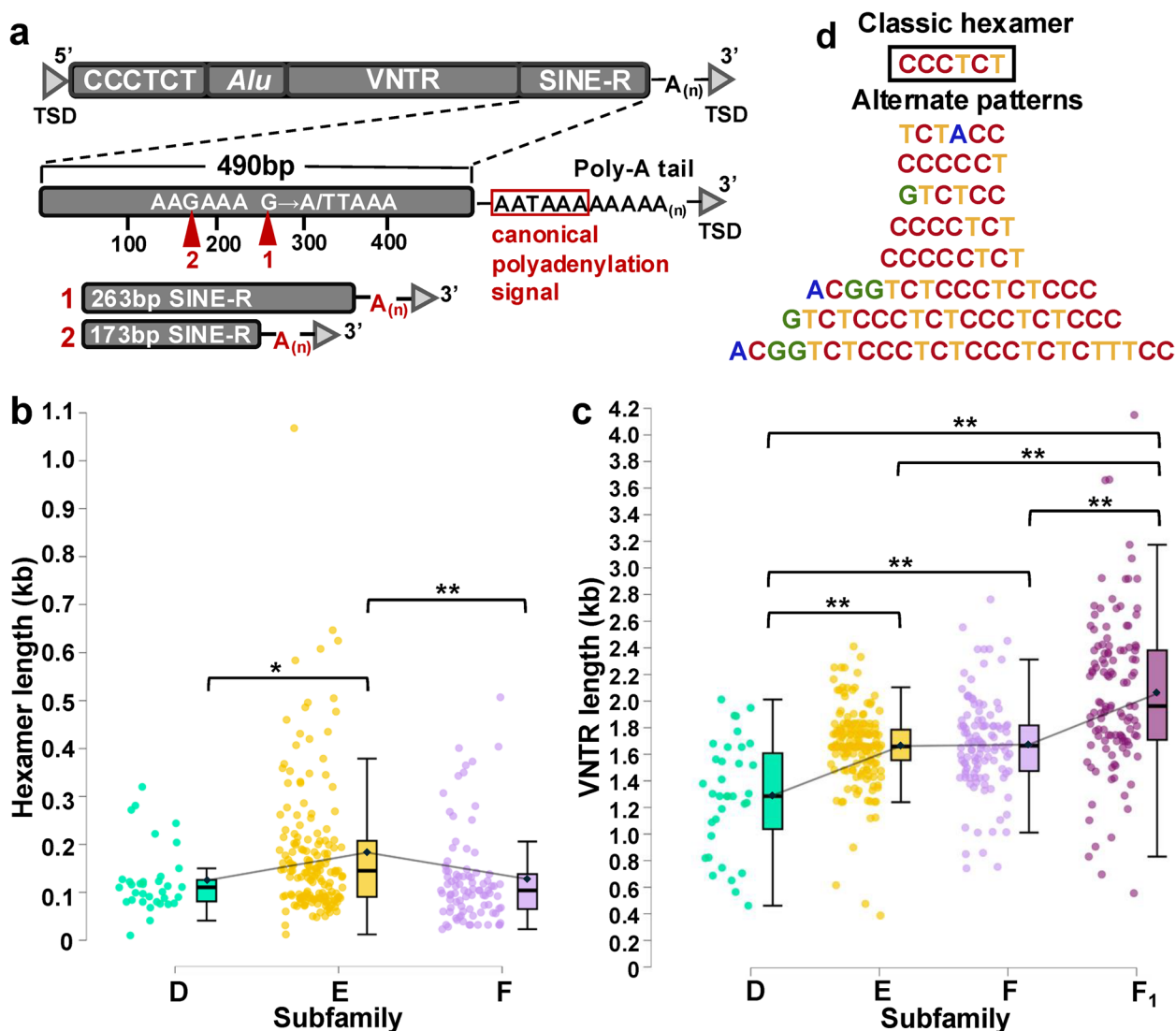


**Fig. 2** SVA structure variation. **a** Visualization of truncation hotspots identified in the SINE-R region. **b** Hexameric length distributions of full-length elements in subfamilies D (M: 125 bp, Mdn: 111 bp,  $p < 0.05$ ), E (M: 183 bp, Mdn: 145 bp,  $p < 0.05$ ), and F (M: 126 bp, Mdn: 104 bp,  $p < 0.01$ ). Post-hoc testing (Tukey's Honest Significant Difference (HSD)) confirmed that SVA\_E hexamers were significantly longer than D ( $p < 0.05$ ) and F ( $p < 0.01$ ) hexamers. **c** VNTR length distributions across subfamilies D-F<sub>1</sub>. The longest VNTRs were observed in SVA\_F<sub>1</sub> (M: 2057 bp, Mdn: 1963 bp), followed by F (M: 1673 bp, Mdn: 1665 bp), E (M: 1662 bp, Mdn: 1659 bp) and D (M: 1290 bp, Mdn: 1285 bp). Pairwise comparison of all subfamilies revealed that VNTR lengths vary significantly across all combinations ( $p < 0.01$ ), with the exception of E and F. However, an increase in mean and median VNTR length from E to F was still observed. Bars denote statistically significant relationships (\*\* $p < 0.01$ , \* $p < 0.05$ ). **d** Comparison between the classically described hexamer and alternate patterns observed in polymorphic elements of subfamilies D-F

patterns are abundant and not of recent, human-specific origin.

#### SVA-mediated transductions

We next investigated SVA-mediated TDs by aligning all non-reference SVA insertions, along with 500 bp of up- and downstream flanking sequence, and scrutinizing the 5' and 3' ends of each SVA for the presence of additional sequence enclosed within TSDs (see *Methods*; Table S4).

While the *MAST2* sequence of SVA\_F<sub>1</sub> is commonly considered a TD [23–25, 32], we regard *MAST2* as a characteristic of the standard SVA\_F<sub>1</sub> structure, given that all SVA\_F<sub>1</sub> elements are likely of single origin, rather than recurrent splicing. Thus, only sequence up- and/or downstream of the F<sub>1</sub> consensus sequence was considered a TD. Each putative TD was queried against GRCh38 using BLAT [37] to determine its source locus and to identify additional putative elements with TDs. We determined

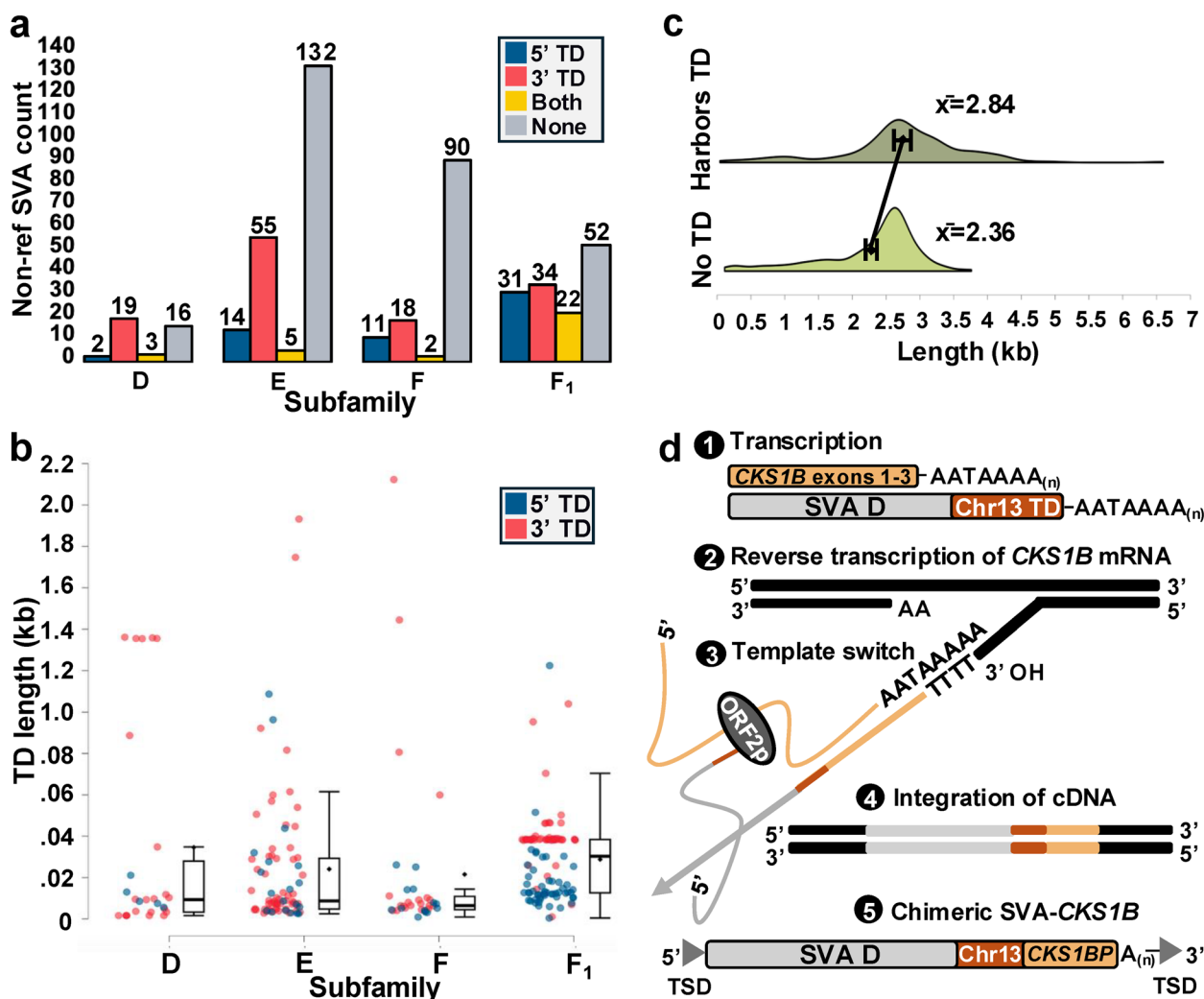


**Fig. 3** SVA-mediated TD events. **a** Number of elements carrying a 5' TD, 3' TD, both, or none across all subfamilies. One additional 5' event, not shown here, is associated with a 5' truncated SVA that could not be differentiated between subfamilies F and F<sub>1</sub>. **b** Distribution of 5' and 3' TD lengths. All TD sequences were separated into 5' and 3' events, with each data point representing a separate event. Investigating subfamily differences, we noted that TDs carried by SVA\_F<sub>1</sub> elements (Mdn: 383 bp) were 3–5× longer than those carried by D (Mdn: 96 bp), E (Mdn: 114 bp) and F (Mdn: 74 bp) elements. **c** Comparison of non-reference SVA lengths with and without TD sequence. **d** Proposed generation mechanism of SVA-*CKS1BP*. 1) Transcription produces *CKS1B* and SVA mRNA. 2) We propose that the *CKS1B* transcript undergoes reverse transcription utilizing the L1 machinery. 3) ORF2p switches from the *CKS1B* transcript to the SVA\_D transcript, and reverse transcription continues through the 5' end of the SVA\_D. 4) The chimeric cDNA product is integrated into the host DNA. 5) The chimeric SVA-*CKS1BP* is a source element, producing additional copies

that 40% (217/543) of the SVA insertions in our dataset harbor a TD. Of these, 58 (27%) carry a 5' TD and 127 (58%) harbor a 3' TD (Fig. 3a; Table S4), indicating that 3' events occur about 2.2× more frequently than 5' events. In addition, we found that 32 (15%) elements have both a 5' and 3' TD (Fig. 3a; Table S4).

Subfamilies exhibited variable TD rates, with 60% (24/40) of D, 36% (74/206) of E, 26% (31/121) of F, and 63% (87/139) of F<sub>1</sub> elements carrying a TD (Fig. S4). While TDs were, on average, 284 bp in length, 3' TDs

were about two-fold longer (M: 347 bp, Mdn: 258 bp) than 5' TDs (M: 172 bp, Mdn: 124 bp), a statistically significant difference (Student's t-test;  $t(230.3) = -4.04$ ,  $p < 0.001$ ) (Fig. 3b). Lengths ranged from 9 bp, to as long as 4 kb. Ultra-short 3' TDs were observed and represent mobilization events of the source element together with its TSD. These events were confirmed through alignment of non-reference insertions to their source element and flanking sequence. Overall, the average length of non-reference SVAs without a TD was 2.36 kb, compared to

2.84 kb for those with a TD (Fig. 3c). Furthermore, we observed that SVAs with a 3' TD generally contained significantly shorter poly-A tails (M: 29.1 bp, Mdn: 26 bp) (ANOVA;  $F(2, 540)=28.48$ ,  $p<0.001$ ), compared to those with a 5' TD (M: 42.1 bp, Mdn: 42.5 bp) or no TD (M: 41.5 bp, Mdn: 39 bp) (Fig. S4).

TDs were traced to all chromosomes, except 18, 21, and Y (Table S4). We identified 27 cases in which TD sequence from multiple source loci was carried by a single SVA (Fig. S5; Table S4), referred to here as concatenated events, demonstrating that offspring elements serve as source elements and that TDs accumulate sequentially [11, 24, 32]. Interestingly, we also observed a TD-only insertion (i.e., absence of SVA), which is caused by premature termination of the reverse transcription process. Such events, deemed “orphan” TDs, have been described for L1 [46], but not for SVA.

### Transduction groups

We next screened all 217 TD-containing SVAs for the presence of shared TD sequence, assigning 68% (149/217) to 25 groups of two or more elements (Table S6). This includes six 5' TD groups encompassing 15 insertions, and 18 3' TD groups containing 69 insertions. In addition, we observed 65 SVA<sub>F1</sub> insertions carrying TD sequence (5' = 15; 3' = 28; both = 22) derived from a locus on chromosome 10, previously associated with 13 SVA<sub>F1</sub> elements in the human reference genome [23–25] (Table S5; Fig. S5). Of these, five represent concatenated events, carrying TDs from chromosomes 8 (3'), 14 ( $n=2$ ; 3'), 17 (both), and 19 (5') in addition to chromosome 10 sequence (Table S5). Based on this, we can infer that chromosome 10-derived SVA<sub>F1</sub> elements have been mobilized by at least six source elements. SVA<sub>F1</sub> elements derived directly or indirectly from chromosome 10 represent, by far, the largest TD group in our dataset, and the only group including insertions with both 5' and 3' shared sequence (Table S5).

One notable 3' TD group included five non-reference elements composed of a full-length SVA<sub>D</sub>, an 87 bp L1M5 fragment, and the VNTR and SINE-R region of a 5' truncated SVA<sub>F</sub> (Fig. S6). A BLAT [37] query of this concatenated SVA against GRCh38 traced the source locus to chromosome 14 (chr14:22,634,849). Further analysis revealed two independent insertions (confirmed by the presence of unique TSDs enclosing each element), with the SVA<sub>D</sub> inserted upstream, and the SVA<sub>F</sub> downstream, of the L1M5 sequence. While the latter sequence is shared with panTro6, the SVA insertions are human specific. The overall higher frequency of 3' TDs, their propensity to be longer than 5' TDs, and the fact that the SVA<sub>D</sub> is full length suggests that the L1M5 and SVA<sub>F</sub> sequences are carried by the SVA<sub>D</sub> as a 3' TD.

### Analysis of transduction sequence

We found that 68% (148/217) of TDs contain TE sequence based on RepeatMasker annotation (Table S7; Fig. S5) [38], including 13% (28/217) with multiple TEs. Most TE sequences represent fragments rather than full-length elements. All [47] chromosome 10-derived SVA<sub>F1</sub> elements include transduced *Alu* sequence on the 5' and/or 3' end, and 64% (14/22) of SVA<sub>F1</sub> TDs not associated with chromosome 10 also harbored some *Alu* sequence. Thus, 91% (79/87) of all SVA<sub>F1</sub> insertions with a TD acquired *Alu* sequence, equating to 70% of SVA<sub>F1</sub> insertions overall. Excluding chromosome 10-derived elements, we find that 68% (36/53) of 5' TDs contain TE sequence, compared to 49% (53/109) of 3' events. Thus, 5' TDs appear to be slightly enriched for TE sequence, while 3' TDs are consistent with the genome background. Furthermore, 5' TDs show ~4× enrichment for *Alu* (21 loci) and ~3× for ERV (14 loci), compared to background proportions. This may suggest that acquisition of SINE and/or LTR sequences on the 5' end is beneficial to transcription and/or propagation. Considering all TDs, TE family composition largely corresponded to the genomic background, with the exception of *Alu*, for which we found an overall enrichment approximately five-fold greater than background levels (Fig. S5).

Analysis of TD source locations revealed that the majority (69%; 150/217) originate within a gene, including 125 protein-coding and 25 non-protein-coding (Table S7), representing a significant enrichment compared to both the total genome composition (based on a proportion of 50.2% genic sequence) [48] (Chi-square test;  $X_2=31.09$ ,  $df=1$ ,  $p<0.001$ ) and the distribution of non-reference insertions in our dataset (Chi-square test;  $X_2=9.195$ ,  $df=1$ ,  $p<0.01$ ). The vast majority of TDs (140; 93%) contain intronic sequence, while ten (7%) map to exonic sequence (Table S7). Of the latter, five are from four protein-coding genes (*CASP8*, *MRPS18A*, *UQCRC1*, and *HGSNAT*), three originate from two antisense long non-coding RNA genes (*TSPAN14-AS1* and *DCTN1-AS1*), and the remaining two map to a long intergenic RNA gene (*LINC02916*) and a close to full-length processed pseudogene (*CKS1BP*) (Fig. 3d). With the exception of *CASP8* and *HGSNAT* [32, 49] (Fig. S7), all other exonic TDs have not been reported.

The three exonic 5' TDs (*LINC02916*, *MRPS18A*, *UQCRC1*) are generated by splicing, either from an exon into an SVA (*MRPS18A*) (Fig. S8), or canonical splicing between exons 1 and 2, followed by readthrough into intron 2 and termination at the 3' end of the SVA (*LINC02916* and *UQCRC1*) (Fig. S9). The *MRPS18A*-containing TD initiates 5 bp upstream of exon 1 and transitions from the end of exon 1 into the SVA at the same splice site within the *Alu* region that gave rise to SVA<sub>F1</sub>

[25], supporting splicing at this position as a recurrent mechanism (Fig. S8). While most 3' TDs (*HGSNAT*, *CASP8* ( $n=2$ ), *TSPAN14-AS1* ( $n=2$ ), *DCTN1-AS1*) are the result of polyadenylation signal readthrough, one insertion (*CKS1BP*) appears to be generated by a different mechanism.

A BLAT [37] query of an 897 bp 3' TD against GRCh38, revealed that 121 bp immediately following the SVA mapped to chromosomes 11 (73,935,481) and 13 (98,030,050), while the 3' end of the TD mapped to eight loci. Of these, seven represent processed pseudogenes, and the remaining locus constitutes the exons of the *CKS1B* gene, beginning at the terminal half of exon 1. First investigating chromosomes 11 and 13, we used RepeatMasker to search for a reference SVA within 5 kb of the 121 bp TD sequence [38]. In doing so, we identified an SVA\_D upstream from the TD sequence on chromosome 11, with 14 bp TSDs enclosing both the SVA and the TD. Based on this, and absence of both at the panTro6 orthologous site, we ruled out chromosome 11 as the origin locus. In contrast, we identified the 121 bp TD sequence on chromosome 13 in both human and chimpanzee, indicating that it is the origin locus. Based on these findings, we infer that an SVA\_D inserted on chromosome 13 but was either lost from the human population or is present at a low allele frequency.

To further investigate the origin of the *CKS1BP* sequence within the 3' TD, we performed an MSA of each *CKS1BP* hit in GRCh38, plus 5 kb bp of up- and downstream flanking sequence [45]. This revealed that two copies, *CKS1BP2* (chr10:29,697,935) and *CKS1BP3* (chr5:62,511,771), harbor SVA\_D elements upstream of the *CKS1BP* sequence and, hence, share the same TD as the non-reference SVA. Mobilization as a unit was further substantiated by the presence of unique TSDs encompassing each SVA and its TD. The five additional processed pseudogenes were neither associated with SVA sequence nor the TD sequence derived from chromosome 11.

To elucidate the origin of the *CKS1BP*-containing SVA elements, we generated a maximum likelihood tree [50, 51] based only on shared sequence across all *CKS1BP* copies and the *CKS1B* mRNA (Fig. S11). Our tree revealed that the non-reference SVA shares the greatest homology with *CKS1BP3*, followed by *CKS1BP2*; and that SVA-associated and non-SVA-associated *CKS1BP* copies form two distinct clades (Fig. S11). Substantiating these relationships, a BLAT query of *CKS1BP* flanking sequences against panTro6, bonobo (panPan3) and gorilla (gorGor6) [37], revealed that only the five non-SVA-associated copies are present at orthologous loci. Thus, the three SVA-associated copies appear to be of more recent, human-specific origin.

Given the absence of a poly-A tail separating the concatenated 3' TD events, the lack of an identifiable splice site (confirmed via manual inspection and a predictive tool [52]), and 5' truncation of the *CKS1B* sequence within the TD, we propose that a template switch from the *CKS1B* mRNA to the SVA mRNA during reverse transcription generated the first SVA-*CKS1BP* copy (Fig. 3d). Based on phylogenetic analysis and sequence scrutiny, we speculate that *CKS1BP2* is the source of our non-reference SVA, which subsequently produced *CKS1BP3*. Support for this includes a short, concatenated 3' TD carried by the non-reference SVA, traced to *CKS1BP2*, as well as unique substitutions shared only between the non-reference insertion and *CKS1BP3*. Our findings demonstrate that SVA-mediated TD represents an alternate pathway for pseudogene propagation.

#### Identification of source elements

Leveraging TD origin coordinates, we searched our non-reference dataset, GRCh38, and T2T-CHM13 for source elements up- or downstream of the TD origin. We identified 9 non-reference source elements in our dataset giving rise to 14 insertions, and 46 additional source elements across GRCh38 and T2T-CHM13 (Fig. 4a-b; Table S8). These 55 source elements gave rise to 183 insertions in our dataset, including 21/25 TD groups and 34/67 singleton events, representing 84% of TD-containing insertions (Table S8). For the remaining insertions, we can infer the origin of the TD despite the absence of an SVA, which may be lost from the population or present at low allele frequency.

We then investigated inter-individual differences in source element abundance across 32 individuals (3 offspring from trios were excluded). Intersecting the insertion coordinates of the 55 identified source elements with the Freeze 4 DEL callset, which encompasses loci that are absent in at least one individual relative to GRCh38, we identified 15 reference source elements that are polymorphic in our individuals. In combination with the nine non-reference source elements identified within our SVA dataset, we uncovered a total of 24 polymorphic source elements, with allele frequencies ranging from 0.016 to 0.95 (M: 0.32, Mdn: 0.38). The remaining 31 reference insertions were homozygous present in all individuals, indicating that they are (nearly) fixed in the human population (Fig. 4b; Table S8).

Of the 55 source SVAs, almost all [53] were present within the AFR population, with the next greatest quantity in the AMR and SAS populations [49], followed by EUR and EAS [48]. Individuals harbored between 37 and 46 source elements, with the highest count observed in two individuals of African ancestry (HG03065 and NA19239) and the lowest in an individual of South Asian

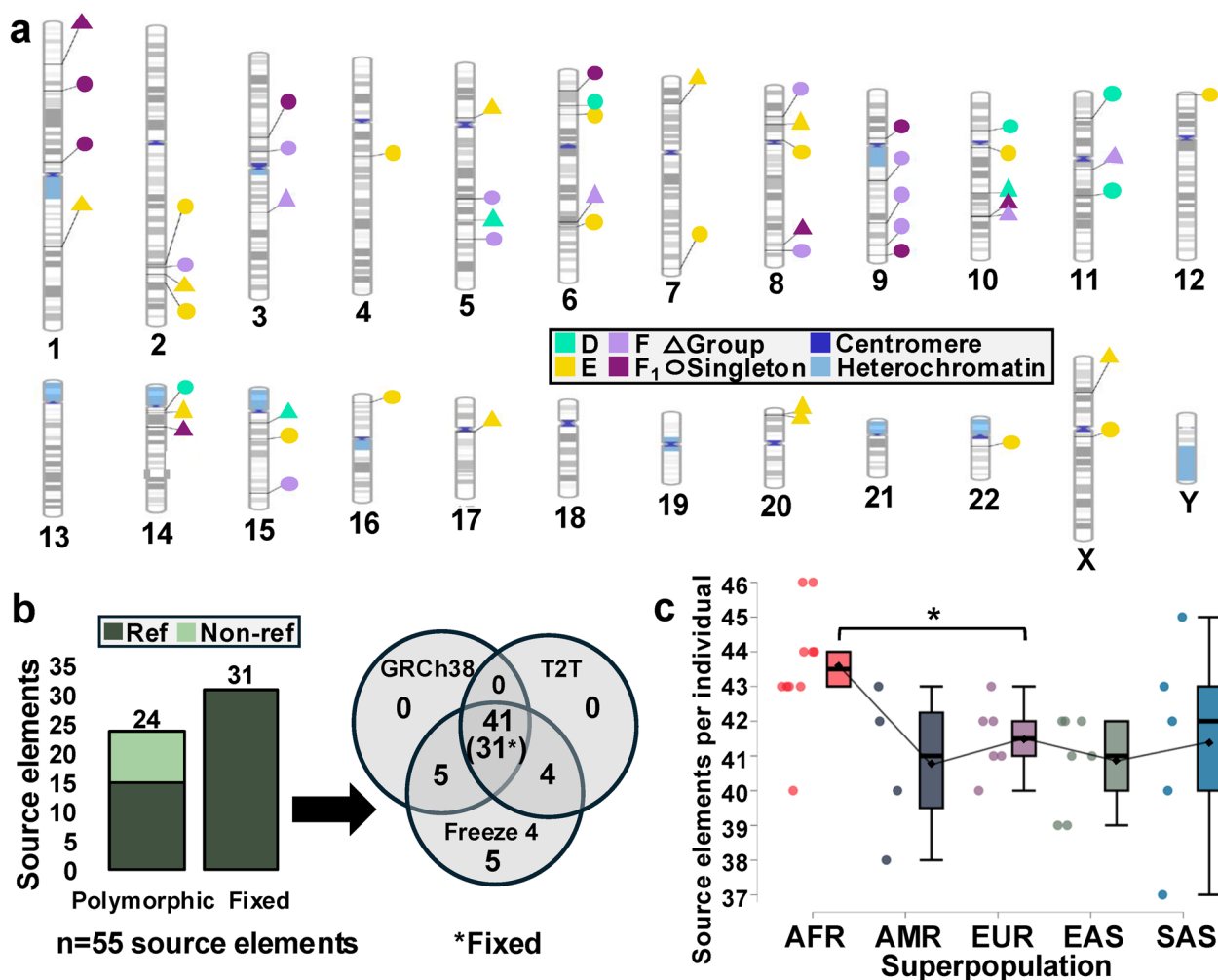


**Fig. 4** SVA TD groups and source elements. **a** Chromosome ideogram depicting loci at which source elements for 21 TD groups (triangles) and 34 singleton TD events (circles) were identified. No source elements were identified on chromosomes 13, 18, 19, 21, or Y. However, the identification of six SVA elements with TDs from chromosome 19 and two from chromosome 13 indicate that there were polymorphic source elements on these chromosomes at some point. **b** Polymorphic and fixed source elements were identified across GRCh38, T2T-CHM13, and the Freeze 4 callset. Reference vs. non-reference refers to presence in GRCh38. **c** Number of source element insertions per individual, including fixed and polymorphic source elements across GRCh38, T2T-CHM13, and Freeze 4. An ANOVA revealed significant variation ( $F(4, 27) = 3.137, p < 0.05$ ) between groups, though AFR and EUR were the only significant pairwise comparison ( $*p < 0.05$ ; Tukey's (HSD))

ancestry (HG03683) (Fig. 4c). Thus, the greatest source element abundance was observed in the AFR superpopulation, on both a population and individual level. Investigating source element subfamily dynamics, we found that 42% were SVA\_E, followed by 25% SVA\_F, 15% SVA\_D, and 18% SVA\_F<sub>1</sub> (Fig. 4a). The relatively low abundance of SVA\_F<sub>1</sub> source elements, despite their overall high TD rate and a propagation rate potentially exceeding SVA\_E, may reflect bias stemming from the grouping of chromosome 10-derived elements. Supporting this, shared sequence features within groups of SVA\_F<sub>1</sub> elements, and concatenated TDs carried by chromosome

10-derived insertions, point to additional unrecovered source elements.

**SVA propagation rate and allele frequency**

Next, we investigated the allele frequencies of 540 non-reference SVA insertions (complete genotype information was unavailable for 3/543) across 32 individuals (offspring from trios were excluded). We observed a mean of 83 non-reference SVA insertions per individual, with the highest and lowest abundance in AFR (M: 94) and EUR (M: 71), respectively (Fig. 5a). Two-thirds (67%; 361/540) of non-reference SVAs had an allele

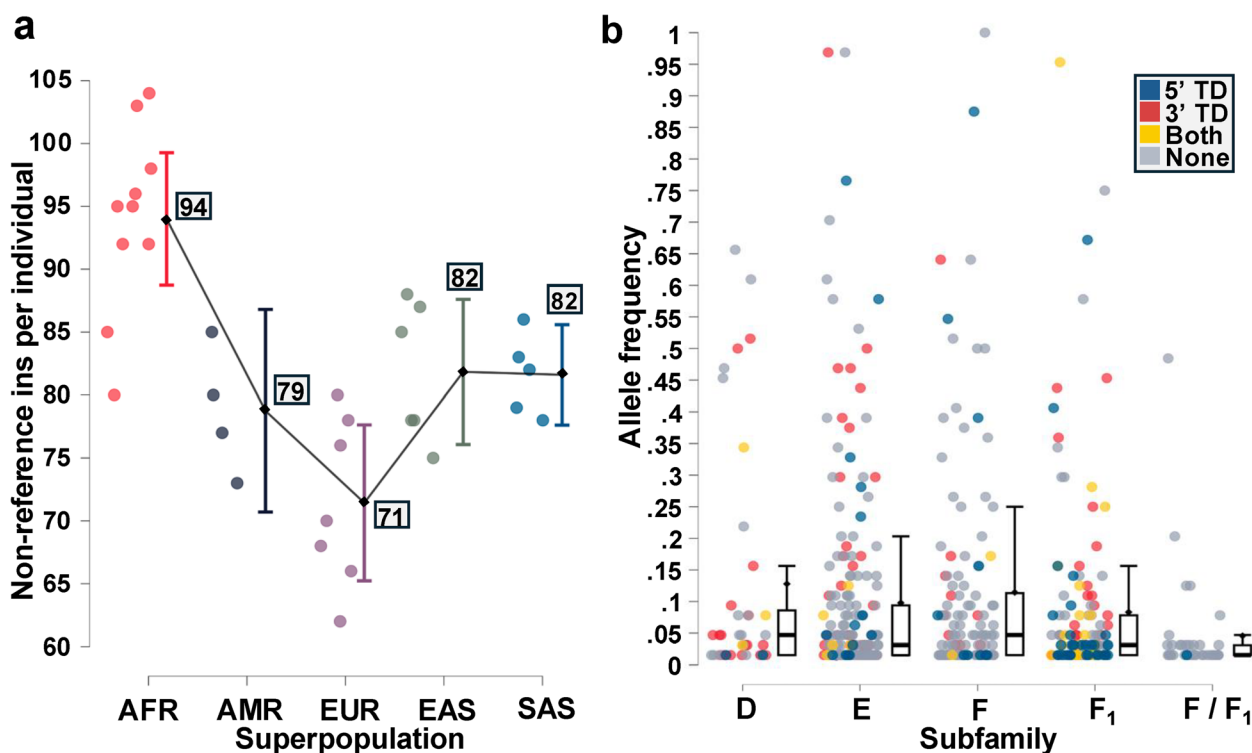


**Fig. 5** Non-reference SVA insertion counts and allele frequencies. **a** SVA propagation differences across 32 individuals (excluding three offspring within trios). The number of non-reference SVA insertions ranged from 62 to 104 (M: 83) per individual. An ANOVA test revealed significant differences in insertion count across superpopulations ( $F(4, 559) = 14.71, p < 0.001$ ), specifically between AFR and all other groups. **b** Allele frequencies for 540 polymorphic insertions across 32 individuals, by subfamily and TD type. Insertions with missing genotypes were excluded. No significant difference in allele frequencies was observed across subfamilies D-F<sub>1</sub> (median D: 0.0468, median E: 0.0313, median F: 0.0468, median F<sub>1</sub>: 0.0313, median F/F<sub>1</sub>: 0.015625). The F/F<sub>1</sub> category refers to the 37 elements that could not be distinguished between F and F<sub>1</sub>

frequency of  $< 0.05$  (M: 0.031, Mdn: 0.096) (Fig. 5b), with 47% (253/540) representing singleton events.

## Discussion

Investigating the genomic distribution of the 543 polymorphic, non-reference SVA elements, we find evidence for non-random insertion, in agreement with previous analyses [12, 16, 18]. In particular, we observe enrichment of insertions into genic sequence, which is in alignment with other studies investigating polymorphic insertions [16, 18]. However, this may be attributed more to the accessibility of open chromatin during SVA mobilization than to targeted insertion into genic regions [18]. In contrast, for reference genome insertions, no such bias was observed [12], indicating that genic insertions may be lost due to negative selection. While we did not find a distribution bias based on allele frequency overall, as expected, the majority (12/14; 86%) of exonic insertions were present at very low allele frequencies (9/14: 1.6%, 3/14: 7.8%). Most (11/14; 79%) exonic SVAs were located in the 3' UTR, in line with findings that insertions occur more frequently than

expected in this region [22, 53, 54]. Such insertions have been associated with reduced expression of protein-coding genes [21, 53].

Also in alignment with previous observations [12], we found that 60% of SVAs are full length and that VNTR length is inversely correlated with evolutionary age. Expansion of the VNTR over time may be the result of polymerase slippage during replication or transcription, or ORF2p slippage during reverse transcription [20], supporting a pattern of expansion rather than contraction. Our fine scale-analyses revealed considerable deviation from the canonical hexameric pattern, with most of the observed patterns likely being introduced prior to the radiation of the human and chimpanzee lineages. Given the hexameric region is suspected to possess promoter activity and has been identified as a source of G-quadruplex formation [13, 18, 55], functional studies exploring whether the observed patterns influence mobilization may provide additional insight into the role of the hexameric region in SVA transcription and retrotransposition.

Our annotation of non-reference SVA insertions across 35 individuals (32 plus 3 offspring) reveals a much higher

mobilization rate of SVA<sub>F1</sub> in the human population than previously appreciated. SVA<sub>F1</sub> represents only a minor fraction of SVA insertions in the human reference genome, with 84 SVAs identified as SVA<sub>F1</sub> (~32% of SVA<sub>F</sub> elements) [24, 25]. In contrast, we identified 139 non-reference SVA<sub>F1</sub> elements across 32 genetically diverse humans, making SVA<sub>F1</sub> more abundant than SVA<sub>F</sub>, based on discernable elements classically annotated as SVA<sub>F</sub>. The enrichment of SVA<sub>F1</sub> among young, polymorphic SVA elements compared to the human reference genome suggests that SVA<sub>F1</sub> is a highly active subfamily, which is also supported by its overall low allele frequency (M: 8%). Thus, SVA<sub>F1</sub> is possibly gaining traction in the human population and may be in the process of outperforming SVA<sub>F</sub>. Taken together, we argue that SVA<sub>F1</sub> should be considered its own subfamily and included in the standard SVA annotation. Further, given the likely origin of SVA<sub>F1</sub> via a single splicing event rather than recurrent splicing, we argue that the *MAST2* sequence should no longer be considered a TD, but part of the standard SVA<sub>F1</sub> structure.

Despite not considering the *MAST2* sequence a TD, we identify more than twice as many TDs compared to previous studies (40% vs. 14–18% with TD) [23–25, 31, 32]. Thus, our SVA<sub>F1</sub> annotation shifts the previously reported predominance of 5' TDs to 3' TDs being more prevalently associated with SVA elements, making it more aligned with L1 insertions, which harbor primarily 3' TDs [28–30]. Further contributing to this is our identification of short 3' TDs that do not appear to result from the use of downstream polyadenylation signals and often represent retention of the parent TSD in the offspring insertion. Though we speculate that these events are attributed to initiation of the poly-A tail downstream from the canonical polyadenylation signal, further investigation into the mechanism is warranted.

While L1-mediated 5' TD events are rare [28], SVA-mediated 5' events are more routinely observed, which may be attributed to differences in promoter usage, as L1 utilizes a well-documented internal promoter [56], yet no such internal promoter has been identified within SVA elements. Rather, both internal and external promoters likely play a role in SVA transcription [10, 13], which may explain their increased acquisition of 5' sequences relative to L1 elements. Interestingly, we find that 91% of 5' TDs in our dataset contain genic sequence and/or SINE and LTR elements, significantly more than would be expected based on the overall genomic distribution of SVA. Thus, we postulate that SVA insertions within these regions may be more active than insertions within other genomic environments, given closer proximity to external promoters, regulatory features, and the transcription machinery are likely beneficial to amplification.

The considerable length variation of the composite SVA structure, which commonly leads to fragmentation of SVAs, combined with the presence of 5' and/or 3' TDs, which can complicate SVA discovery, are likely contributing factors of SVA underascertainment. Thus, implementation of SVA<sub>F1</sub> annotation into standard repeat analyses and accurate annotation of TDs may likely improve SVA insertion discovery. For example, determination of TSDs combined with a BLAT query of any non-SVA sequence within TSDs, led to the discovery of very short TDs, which often represent the TSDs of the source element, as well as very long, concatenated sequences.

Our analyses further support acquisition of TD sequence through initiation of transcription at upstream start sites, readthrough of the 3' end, and alternative splicing into the SVA [23–25]. In addition, our analyses reveal template switch between a processed pseudogene and an SVA, as well as canonical splicing of a long non-coding RNA, followed by readthrough into the SVA, as additional mechanisms for SVA-mediated TD. Our findings of exonic TDs and the mobilization of a processed pseudogene further elucidate the role of SVA in genome-shaping events, such as exon shuffling and gene duplication [25, 31].

Previously, the 3' *Alu* TD associated with many chromosome 10-derived SVA<sub>F1</sub> elements was shown to increase its mobilization by 25-fold, compared to chromosome 10-derived SVA<sub>F1</sub> elements only carrying the 5' *Alu* TD [13]. Here, we demonstrate that the majority (70%) of all SVA<sub>F1</sub> insertions, including those not associated with chromosome 10, have acquired some *Alu* sequence via a TD, supporting that inclusion may be advantageous for retrotransposition. The overrepresentation could be a consequence of the ability of *Alu* elements to capture L1 proteins at the ribosome, subsequently promoting retrotransposition [8, 57, 58] and a compensatory mechanism in response to replacement of the majority of the internal *Alu* region by *MAST2* [24]. In alignment with this, we found that only 18% of SVA<sub>D-F</sub> elements carrying a TD had acquired *Alu* sequence (representing ~6% of all D-F elements in our dataset).

We also observed SVA-mediated mobilization of exonic sequence, and even of a close to full-length *CKS1B* processed pseudogene. Based on the divergence from the *CKS1B* gene combined with presence in chimpanzee, we can infer that the five non-SVA associated *CKS1BP* reference copies represent separate insertion events of processed pseudogenes mediated by the enzymatic machinery of L1. In contrast, the pattern of the three human-specific SVA-associated processed pseudogenes suggests a single origin event, followed by mobilization as an SVA-TD-processed pseudogene unit. Interestingly,

*CKS1BP7*, a non-SVA-associated copy, is expressed in about a third of breast cancer tumors [59], and overexpression of the *CKS1B* parent gene is associated with aggressive progression and poor prognosis in a number of cancers [47, 60–66].

We also identified two SVA elements carrying a 3' TD of *CASP8* exonic sequence in antisense orientation. One of these, along with an additional polymorphic insertion carrying the *CASP8* TD, had been previously identified in the Icelandic population. The source SVA element, which is present in GRCh38 and located in intron 8 of the *CASP8* gene, has been associated with aberrant splicing and intron retention [49]. Furthermore, this insertion has been associated with breast cancer and basal cell carcinoma occurrence, as well as protection against prostate cancer [49]. Finally, we identified an orphan TD, wherein the TD sequence was identified without an adjacent SVA, likely as a result of extreme 5' truncation during reverse transcription. A pathogenic L1-mediated orphan TD was previously identified as the causative variant in Duchenne muscular dystrophy [46], demonstrating that such insertions have mutagenic potential.

We identified active, polymorphic source elements for all propagating subfamilies (D-F<sub>1</sub>), supporting recent activity, or even continuing propagation, in the human population and shedding light on elements with the highest potential for generating de novo insertions. We found that individuals possess between 37–46 source elements, likely an underestimation given our analysis was based solely on source elements producing TDs. Such differences in source element abundance lead to inter-individual variation in SVA propagation rates, contributing to genetic variation, evidenced by our finding that individuals possess between 62–104 total non-reference insertions. Ongoing mobilization of subfamilies D-F<sub>1</sub> is further supported by the identification of at least 28 insertions causing monogenic disorders [21], and the impact of SVA on phenotypic variation, such as skin pigmentation loss in European populations [67].

Interestingly, SVA\_E comprised the greatest proportion of identified source elements (42%), and of all non-reference insertions (38%; 206/543), despite comprising only ~4.4% of reference SVAs [12], suggesting that SVA\_E is actively propagating, with potentially the highest propagation rate. The low abundance in the human reference genome may indicate a recent increase in propagation. Alternatively, SVA\_E may underlie strong negative selection. In contrast, SVA\_D comprised 15% of source elements and 7% (40/543) of non-reference insertions, despite representing ~43% of reference SVAs [12], suggesting that this evolutionarily older subfamily is currently mobilizing at far lower rates than in the past.

We identified ten SVA\_F<sub>1</sub> source elements. Of these, two, including the chromosome 10 master source and a non-reference, polymorphic source on chromosome 14, produced offspring with chromosome 10-derived TDs. Thus, we provide evidence that offspring produced by the chromosome 10 master locus are also retrotransposition competent. SNVs shared among small groups of chromosome 10-derived elements, and SVA\_F<sub>1</sub> elements carrying concatenated TDs, point to additional, unrecovered source elements that have likely been lost from the population. Given this, we speculate that the F<sub>1</sub> element on chromosome 10 may be a “stealth driver,” giving rise to short-lived, but highly active, insertions that are quickly lost from the population, as previously described for *Alu* [12, 68]. The comparable number of identified F and F<sub>1</sub> source elements (14 and 10, respectively), in conjunction with the potential for unrecovered F<sub>1</sub> source elements, provides support for our hypothesis that F<sub>1</sub> is currently propagating at levels on par with, and potentially exceeding, SVA\_F.

## Conclusion

Here, we provide insight into the youngest, polymorphic SVA elements currently propagating in the human population. Our analyses reveal that the evolutionary youngest subfamily, SVA\_F<sub>1</sub>, is establishing itself as a main driver of SVA expansion in the human population. Based on this abundance, we strongly argue that SVA\_F<sub>1</sub> has reached subfamily status. Further, we discovered that the overall SVA-mediated TD rate is two-fold higher than previously estimated, and that 3' events are more abundant than 5' events in our dataset. We highlight the wide range of mechanisms contributing to TD events beyond upstream promoter usage (leading to 5' TD) and 3' polyadenylation signal readthrough, such as template switch. Leveraging TD sequences, we trace 84% of TD-containing elements to 55 active source elements and highlight variation in source element abundance on an individual and population level.

## Methods

### SVA identification

A local installation of RepeatMasker (v4.1.6) [38] with the Dfam (v3.8) [44] library was run on the HGSCV Freeze 4 merged SV callset. The RepeatMasker.out file and a Fasta file containing all SV sequences were provided to L1ME-AID (v1.0.0-beta) [36] (<https://github.com/MarkIoftus/L1ME-AID>), a pipeline which identifies TEs based on presence of non-LTR retrotransposon sequence (*Alu*, L1, SVA), a poly-A tail, and semi-low divergence (*Alu*: <6%, L1/SVA: <15%) compared to the Dfam consensus sequence [44]. SVAs were then filtered out, producing 583 putative elements. To manually curate, 500 bp

of flanking sequence up- and downstream of each insertion coordinate was pulled from the assemblies and used to confirm endonuclease cleavage sites, TSDs and poly-A tails. Flanking sequences were also queried against GRCh38 to confirm the absence of each SVA from the reference genome [37]. Ultimately, 40 putative loci were removed in accordance with our established parameters, resulting in a final high-confidence dataset of 543 non-reference SVAs.

### Sequence analyses

All sequence alignments were generated using MUSCLE (v3.8.31) [45] and visualized in AliView (v1.27) (<https://github.com/AliView/AliView>) [69].

### Statistical analyses

JASP software (v0.19.3) (<https://github.com/jasp-stats>) [70] was used to perform statistical analyses, including: Chi-square Goodness-of-Fit test, ANOVA with Tukey's Honest Significant Difference post-hoc test, and Independent Samples T-test. Figures 2b-c, 3b, 4c, and 5a-b were generated using JASP [70].

### Phylogenetic tree generation

MSAs were generated using MUSCLE (v3.8.31) [45] and resultant alignments were input into raxmlGUI 2.0 (v2.0.15) [50] to generate maximum likelihood trees (<https://antonellilab.github.io/raxmlGUI/>). Phylogenetic trees were visualized using FigTree (v1.4.4) [51] (<https://github.com/rambaut/figtree>).

### Genomic distribution

A Chi-square Goodness-of-Fit test was performed to compare the observed (based on non-reference SVA insertion coordinates) and expected distribution of SVA elements. Expected counts were calculated by dividing each chromosome length by the total size of GRCh38 [71], and multiplying the resultant proportion by 543.

To determine if SVAs were inter- or intragenic, insertion coordinates for all 543 non-reference elements were intersected with GENCODE gene information (v46lift37) [39] and visualized on the UCSC Genome Browser (GRCh38). A Chi-square Goodness-of-Fit test was performed based on a genomic proportion of 41% (~40% intronic and ~1% exonic) protein-coding genes [40]. Exonic insertions were further scrutinized to determine insertion into coding sequence or UTRs (GENCODE v46lift37) [39]. The RepeatMasker (v3.0.1) [38] track of the UCSC Genome Browser (GRCh38) was used to evaluate insertion sites for presence of TEs.

### Subfamily annotation

SVAs were first grouped into subfamily bins (e.g., SVA D/E/F) based on RepeatMasker (v4.1.6; Dfam v3.8) annotation [38, 44]. Next, an MSA was generated for each subfamily bin, and SVA sequences were scrutinized for any deviation from the established (Dfam) consensus sequence. SVA\_F elements containing *MAST2* exon 1 sequence on their 5' ends (confirmed via a BLAT search against GRCh38 [37]) were filtered from the SVA\_F group and used to generate an SVA\_F<sub>1</sub> subfamily-specific alignment.

### Structural analyses

For subfamilies D-F, full length was defined as the presence of at least one hexameric repeat on the 5' end and a poly-A tail following a complete SINE-R region on the 3' end. For SVA\_F<sub>1</sub>, full length was defined as >320 bp of *MAST2* sequence on the 5' end, based on the distance from the *MAST2*/SVA splice junction to the beginning of the first hexameric repeat relative to the SVA\_F consensus sequence, and a poly-A tail following a full SINE-R region on the 3' end (Fig. 2). SVAs initiating or terminating at an alternate point compared to the subfamily consensus sequence were classified as 5' and/or 3' truncation events, and the region of truncation (e.g., SINE-R) was recorded.

To investigate subfamily differences, the hexameric (SVA\_D-F), VNTR (SVA\_D-F<sub>1</sub>), and poly-A tail (SVA\_D-F<sub>1</sub>) regions were analyzed. To capture the broad pattern variability in the hexameric region, all observed patterns were included, given at least one repeat unit was present. For the VNTR analysis, only insertions with a full-length (i.e., not truncated within the region) VNTR were included. To determine poly-A tail lengths, the terminal polyadenylation signal was identified, and the downstream poly-A tail was quantified through the last nucleotide preceding the 3' TSD.

### Identification and analysis of transductions

All non-reference SVA insertions, plus 500 bp of up- and downstream flanking sequence, were aligned and screened for the presence of sequence 5' and/or 3' of the consensus, enclosed within TSDs. Each sequence was manually scrutinized to facilitate identification of the shortest TDs. Putative TD sequences were used as a BLAT [37] query against GRCh38 to identify the origin locus. BLAT hits were filtered by percent identity, and absence of a poly-A tail following the sequence match at the putative origin site was confirmed. GENCODE (v46lift37) [39] and RepeatMasker (v3.0.1) [38] annotations of GRCh38 were used to determine if TD sequences were genic and/or contained TE sequences. Sequence from each putative origin site was retrieved

from GRCh38 and aligned with the corresponding non-reference TD sequence to further validate the source locus and determine the exact length of the matching sequence. In some cases, one SVA carried multiple TD sequences traced to different source loci, deemed “concatenated TDs.” These were counted as one event for the overall TD rate, although each separate TD within was recorded. Two or more SVAs with shared TD sequence were sorted into groups. A Chi-square Goodness-of-Fit test was performed to determine if TDs originate in genes more frequently than expected, based on a total genomic proportion of 50.2% genic (protein- and non-protein-coding) sequence [48].

### Source elements

To identify retrotranspositionally active SVA insertions (i.e., source elements), the RepeatMasker track (v3.0.1) [38] of the UCSC Genome Browser (GRCh38) was used to determine presence of a reference SVA element up-or downstream of each TD origin site. The T2T (CHM13v2.0/hs1) assembly was then queried to locate additional source SVAs absent from GRCh38. Finally, TD origin coordinates were screened against all non-reference SVA insertion coordinates to identify non-reference elements serving as source elements. All candidate source elements were confirmed via identification of source TSDs within the TD sequence. A chromosome ideogram was generated based on source element insertion coordinates (GRCh38), using the PhenoGram graphical interface (<https://visualization.ritchielab.org/phenoGrams/plot>) [72].

Next, coordinates of the identified source elements were screened against the Freeze 4 DEL callset, which contains loci absent in at least one individual relative to GRCh38 (i.e. polymorphic source elements). For all elements located in the Freeze 4 DEL callset, sequences were aligned to the corresponding source SVA sequence downloaded from the UCSC Genome Browser (GRCh38) for validation, and were classified as polymorphic. Identified source elements absent from the Freeze 4 DEL callset were classified as fixed.

To determine if source elements were enriched within protein-coding genic regions (i.e., insertions in introns), a Chi-square Goodness-of-Fit test was performed. The proportion of the genome composed of protein-coding genes (0.41, including 40% intronic sequence and 1% exonic sequence) [40] was multiplied by the number of non-reference SVAs (543) to calculate expected counts.

### Allele frequencies

Offspring from three parent–child trios (HG00514, HG00733, NA19240) were excluded, and complete genotype information was available for 540/543 SVAs. Allele

frequencies were calculated by adding all alleles present for any given insertion and dividing by total number of alleles ( $n = 64$ ).

### Abbreviations

BLAT	BLAST-like alignment tool
bp	Base pairs
HGSVC	Human Genome Structural Variation Consortium
indel	Insertion/deletion
kb	Kilobase
L1ME-AID	L1 Mediated Annotation and Insertion Detector
LINE	Long interspersed element
MSA	Multiple sequence alignment
MUSCLE	Multiple sequence comparison by log-expectation
NMD	Nonsense-mediated decay
SINE	Small interspersed element
SINE-R	SVA region derived from the 3' end of the <i>env</i> gene and 3' LTR of HERVK-10
SNV	Single nucleotide variant
SVA	SINE variable number tandem repeat <i>Alu</i>
TD	Transduction
TE	Transposable element
TSD	Target site duplication
UTR	Untranslated region
VNTR	Variable number tandem repeat

### Supplementary Information

The online version contains supplementary material available at <https://doi.org/10.1186/s13100-025-00373-w>.

Supplementary Material 1.

Supplementary Material 2.

### Acknowledgements

We thank all members of the Konkel laboratory for their critical discussion and valuable feedback. We thank the HGSVC for providing access to the genome assemblies and structural variant data utilized in this study. The HGSVC included as a co-author in this manuscript includes the following authors (alphabetical order except for chairs): Haley J Abel, Hufsa Ashraf, Peter A Audano, Anna O Basile, Marc Jan Bonder, Harrison Brand, Marta Byrska-Bishop, Mark JP Chaisson, Junjie Chen, Yu Chen, Zechen Chong, Nelson T Chuang, Wayne E Clarke, André Corvelo, Scott E Devine, Peter Ebert, Jana Ebler, Uday S Evani, Susan Fairley, Paul Flicek, Mark B Gerstein, Maryam Ghareghani, Ira M Hall, William T Harvey, Patrick Hasenfeld, Alex R Hastie, Wolfram Höps, PingHsun Hsieh, Sushant Kumar, Joyce Lee, Alexandra P Lewis, Chong Li, Yang I Li, Jiadong Lin, Tsung-Yu Lu, Rebecca Serra Mari, Ryan E Mills, Zepeng Mu, Katherine M Munson, David Porubsky, Benjamin Raeder, Tobias Rausch, Allison A Regier, Jingwen Ren, Bernardo Rodriguez-Martin, Ashley D Sanders, Martin Santamarina, Xinghua Shi, Oliver Stegle, Arvis Sulovari, Michael E Talkowski, Luke J Tallon, Jose MC Tubio, Aaron M Wenger, Xiaofei Yang, Kai Ye, Feyza Yilmaz, Xuefang Zhao, Weichen Zhou, Qihui Zhu, Michael C Zody, Jan O Korbel, Tobias Marschall, Evan E Eichler, and Charles Lee.

### Authors' contributions

AEK, ML, ECG, and MKK performed data analyses. AEK prepared figures and supplemental materials. AEK and MKK conceptualized the project and designed the analyses. AEK and MKK wrote the manuscript. AEK, ML, and MKK edited the manuscript. MKK secured funding for the project. The Freeze 4 SV callset was generated by the HGSVC. All authors have read and agreed to the published version of the manuscript.

### Funding

Open access funding provided by the Carolinas Consortium. This work was supported by the Center for Biomedical Research Excellence (COBRE) in Human Genetics grant P20GM139769, awarded to the Clemson University Center for Human Genetics by the National Institute of General Medical Sciences of the National Institutes of Health (NIH). This project was also partially

supported by the Clemson University Creative Inquiry program. Parts of this research used resources on the Palmetto Cluster at Clemson University under National Science Foundation awards MRI 1228312, II NEW 1405767, MRI 1725573, and MRI 2018069. The HGSVC was supported by the NIH National Human Genome Research Institute grant U24HG007497. The views expressed in this article do not necessarily represent the views of NSF, NIH, or the United States government.

#### Data availability

Data generated by the HGSVC2 is publicly available on the online portal: <https://www.internationalgenome.org/data-portal/data-collection/hgsvc2>. The dataset generated and analyzed during this study is included within the supplementary material.

#### Declarations

#### Ethics approval and consent to participate

Not applicable.

#### Consent for publication

Not applicable.

#### Competing interests

The authors declare no competing interests.

Received: 6 August 2025 Accepted: 1 September 2025

Published online: 06 November 2025

#### References

- Wells JN, Feschotte C. A field guide to eukaryotic transposable elements. *Annu Rev Genet.* 2020;54:539–61.
- Lander ES, Linton LM, Birren B, Nusbaum C, Zody MC, Baldwin J, et al. Initial sequencing and analysis of the human genome. *Nature.* 2001;409(6822):860–921.
- de Koning APJ, Gu W, Castoe TA, Batzer MA, Pollock DD. Repetitive elements may comprise over two-thirds of the human genome. *PLoS Genet.* 2011;7(12):e1002384.
- Wheeler TJ, Clements J, Eddy SR, Hubley R, Jones TA, Jurka J, et al. Dfam: a database of repetitive DNA based on profile hidden Markov models. *Nucleic Acids Res.* 2013;41:D70–82.
- Smit AFA. Interspersed repeats and other mementos of transposable elements in mammalian genomes. *Curr Opin Genet Dev.* 1999;9(6):657–63.
- Belancio VP, Hedges DJ, Deininger P. Mammalian non-LTR retrotransposons: for better or worse, in sickness and in health. *Genome Res.* 2008;18(3):343–58.
- Konkel MK, Walker JA, Batzer MA. LINEs and SINEs of primate evolution. *Evol Anthropol.* 2010;19(6):236–49.
- Dewannieux M, Esnault C, Heidmann T. LINE-mediated retrotransposition of marked Alu sequences. *Nat Genet.* 2003;35(1):41–8.
- Ostertag EM, Kazazian HHJ. Biology of mammalian L1 retrotransposons. *Annu Rev Genet.* 2001;35:501–38.
- Hancks DC, Goodier JL, Mandal PK, Cheung LE, Kazazian HHJ. Retrotransposition of marked SVA elements by human L1s in cultured cells. *Hum Mol Genet.* 2011;20(17):3386–400.
- Ostertag EM, Goodier JL, Zhang Y, Kazazian HHJ. SVA elements are non-autonomous retrotransposons that cause disease in humans. *Am J Hum Genet.* 2003;73(6):1444–51.
- Wang H, Xing J, Grover D, Hedges DJ, Han K, Walker JA, Batzer MA. SVA elements: A hominid-specific retroposon family. *J Mol Biol.* 2005;354(4):994–1007.
- Raiz J, Damert A, Chira S, Held U, Klawitter S, Hamdorf M, et al. The non-autonomous retrotransposon SVA is trans-mobilized by the human LINE-1 protein machinery. *Nucleic Acids Res.* 2012;40(4):1666–83.
- Schramm L, Hernandez N. Recruitment of RNA polymerase III to its target promoters. *Genes Dev.* 2002;16(20):2593–620.
- Strichman-Almashanu LZ, Lee RS, Onyango PO, Perlman E, Flam F, Friedman MB, et al. A genome-wide screen for normally methylated human CpG islands that can identify novel imprinted genes. *Genome Res.* 2002;12(4):543–54.
- Gianfrancesco O, Geary B, Savage AL, Billingsley KJ, Bubbs VJ, Quinn JP. The role of SINE-VNTR-Alu (SVA) retrotransposons in shaping the human genome. *Int J Mol Sci.* 2019. <https://doi.org/10.3390/ijms20235977>.
- Horváth V, Garza R, Jönsson ME, Johansson PA, Adami A, Christoforidou G, et al. Mini-heterochromatin domains constrain the cis-regulatory impact of SVA transposons in human brain development and disease. *Nat Struct Mol Biol.* 2024. <https://doi.org/10.1038/s41594-024-01320-8>.
- Savage AL, Bubbs VJ, Breen G, Quinn JP. Characterisation of the potential function of SVA retrotransposons to modulate gene expression patterns. *BMC Evol Biol.* 2013;13(1):101.
- Bochman ML, Paeschke K, Zakian VA. DNA secondary structures: stability and function of G-quadruplex structures. *Nat Rev Genet.* 2012;13(11):770–80.
- Hancks DC, Kazazian HH. SVA retrotransposons: evolution and genetic instability. *Semin Cancer Biol.* 2010;20(4):234–45.
- Pfaff AL, Singleton LM, Köks S. Mechanisms of disease-associated SINE-VNTR-Alus. *Exp Biol Med.* 2022;247(9):756–64.
- Kwon YJ, Choi Y, Eo J, Noh YN, Gim JA, Jung Y, et al. Structure and expression analyses of SVA elements in relation to functional genes. *Genomics Inform.* 2013;11:142–8.
- Bantysh OB, Buzdin AA. Novel family of human transposable elements formed due to fusion of the first exon of gene MAST2 with retrotransposon SVA. *Biochemistry.* 2009;74(12):1393–9.
- Damert A, Raiz J, Horn AV, Löwer J, Wang H, Xing J, et al. 5'-transducing SVA retrotransposon groups spread efficiently throughout the human genome. *Genome Res.* 2009;19(11):1992–2008.
- Hancks DC, Ewing AD, Chen JE, Tokunaga K, Kazazian HHJ. Exon-trapping mediated by the human retrotransposon SVA. *Genome Res.* 2009;19(11):1983–91.
- Xing J, Zhang Y, Han K, Salem AH, Sen SK, Huff CD, et al. Mobile elements create structural variation: analysis of a complete human genome. *Genome Res.* 2009;19(9):1516–26.
- Feusier J, Watkins WS, Thomas J, Farrell A, Witherspoon DJ, Baird L, et al. Pedigree-based estimation of human mobile element retrotransposition rates. *Genome Res.* 2019;29(10):1567–77.
- Moran JV, DeBerardinis RJ, Kazazian HH. Exon shuffling by L1 retrotransposition. *Science.* 1999;283(5407):1530–4.
- Pickeral OK, Makalowski W, Boguski MS, Boeke JD. Frequent human genomic DNA transduction driven by LINE-1 retrotransposition. *Genome Res.* 2000;10(4):411–5.
- Goodier JL, Ostertag EM, Kazazian HH Jr. Transduction of 3'-flanking sequences is common in L1 retrotransposition. *Hum Mol Genet.* 2000;9(4):653–7.
- Xing J, Wang H, Belancio VP, Cordaux R, Deininger PL, Batzer MA. Emergence of primate genes by retrotransposon-mediated sequence transduction. *Proc Natl Acad Sci USA.* 2006;103(47):17608–13.
- Ebert P, Audano PA, Zhu Q, Rodriguez-Martin B, Porubsky D, Bonder MJ, et al. Haplotype-resolved diverse human genomes and integrated analysis of structural variation. *Science.* 2021. <https://doi.org/10.1126/science.abf7117>.
- Chu C, Lin EW, Tran A, Jin H, Ho NI, Veit A, et al. The landscape of human SVA retrotransposons. *Nucleic Acids Res.* 2023;51(21):11453–65.
- Kidd JM, Graves T, Newman T, Fulton R, Hayden HS, Malig M, et al. A human genome structural variation sequencing resource reveals insights into mutational mechanisms. *Cell.* 2010;143(5):837–47.
- Beck CR, Garcia-Perez JL, Badge RM, Moran JV. LINE-1 elements in structural variation and disease. *Annu Rev Genomics Hum Genet.* 2011;12(1):187–215.
- Logsdon GA, Ebert P, Audano PA, Loftus M, Porubsky D, Ebler J, et al. Complex genetic variation in nearly complete human genomes. *Nature.* 2025;644(8076):430–441.
- Kent WJ. BLAT—The BLAST-Like Alignment Tool. *Genome Res.* 2002;12(4):656–64.
- Smit AFA, Hubley R, Green P. RepeatMasker Open-4.0. 2013–2015. Available from: <https://www.repeatmasker.org>.
- Frankish A, Diekhans M, Ferreira AM, Johnson R, Jungreis I, Loveland J, et al. GENCODE reference annotation for the human and mouse genomes. *Nucleic Acids Res.* 2019;47(D1):D766–73.

40. Hatje K, Mühlhausen S, Simm D, Kollmar M. The protein-coding human genome: annotating high-hanging fruits. *BioEssays*. 2019. <https://doi.org/10.1002/bies.201900066>.
41. Stewart C, Kural D, Strömberg MP, Walker JA, Konkol MK, Stütz AM, et al. A comprehensive map of mobile element insertion polymorphisms in humans. *PLoS Genet*. 2011;7(8):e1002236.
42. Nagy E, Maquat LE. A rule for termination-codon position within intron-containing genes: when nonsense affects RNA abundance. *Trends Biochem Sci*. 2025;23(6):198–9.
43. Lykke-Andersen S, Jensen TH. Nonsense-mediated mRNA decay: an intricate machinery that shapes transcriptomes. *Nat Rev Mol Cell Biol*. 2015;16(11):665–77.
44. Storer J, Hubley R, Rosen J, Wheeler TJ, Smit AF. The dfam community resource of transposable element families, sequence models, and genome annotations. *Mob DNA*. 2021;12(1):2.
45. Edgar RC. MUSCLE: multiple sequence alignment with high accuracy and high throughput. *Nucleic Acids Res*. 2004;32(5):1792–7.
46. Solyom S, Ewing AD, Hancs DC, Takeshima Y, Awano H, Matsuo M, et al. Pathogenic orphan transduction created by a nonreference LINE-1 retrotransposon. *Hum Mutat*. 2012;33(2):369–71.
47. Shaughnessy J. Amplification and overexpression of *CKS1B* at chromosome band 1q21 is associated with reduced levels of p27 Kip1 and an aggressive clinical course in multiple myeloma. *Hematology*. 2005;10(sup1):117–26.
48. Francis WR, Wörheide G. Similar ratios of introns to intergenic sequence across animal genomes. *Genome Biol Evol*. 2017;9(6):1582–98.
49. Stacey SN, Kehr B, Gudmundsson J, Zink F, Jonasdottir A, Gudjonsson SA, et al. Insertion of an SVA-E retrotransposon into the *CASP8* gene is associated with protection against prostate cancer. *Hum Mol Genet*. 2016;25(5):1008–18.
50. Edler D, Klein J, Antonelli A, Silvestro D. RaxmlGUI 2.0: a graphical interface and toolkit for phylogenetic analyses using RAXML. *Methods Ecol Evol*. 2021;12(2):373–7.
51. Rambaut A. FigTree v1.4.4. Edinburgh: Institute of Evolutionary Biology, University of Edinburgh; 2018. Available from: <https://tree.bio.ed.ac.uk/software/figtree/>.
52. Wang M, Marin A. Characterization and prediction of alternative splice sites. *Gene*. 2006;366(2):219–27.
53. Faulkner GJ, Kimura Y, Daub CO, Wani S, Plessy C, Irvine KM, et al. The regulated retrotransposon transcriptome of mammalian cells. *Nat Genet*. 2009;41(5):563–71.
54. Savage AL, Iacoangeli A, Schumann GG, Rubio-Roldan A, Garcia-Perez JL, Al Khleifat A, et al. Characterisation of retrotransposon insertion polymorphisms in whole genome sequencing data from individuals with amyotrophic lateral sclerosis. *Gene*. 2022;843:146799.
55. Nicoletto G, Terreri M, Maurizio I, Ruggiero E, Cernilogar FM, Vaine CA, et al. G-quadruplexes in an SVA retrotransposon cause aberrant *TAF1* gene expression in X-linked dystonia parkinsonism. *Nucleic Acids Res*. 2024;52(19):11571–86.
56. Swergold GD. Identification, characterization, and cell specificity of a human LINE-1 promoter. *Mol Cell Biol*. 1990;10(12):6718–29.
57. Boeke JD. LINES and Alus — the polyA connection. *Nat Genet*. 1997;16(1):6–7.
58. Mills RE, Bennett EA, Iskow RC, Devine SE. Which transposable elements are active in the human genome? *Trends Genet*. 2007;23(4):183–91.
59. Liu Y, Wang W, Li Y, Sun F, Lin J, Li L. *CKS1BP7*, a pseudogene of *CKS1B*, is co-amplified with *IGF1R* in breast cancers. *Pathol Oncol Res*. 2018;24(2):223–9.
60. Liu X, Zhao D. *CKS1B* promotes the progression of hepatocellular carcinoma by activating *JAK/STAT3* signal pathway. *Anim Cells Syst*. 2021;25(4):227–34.
61. Fujita Y, Yagishita S, Hagiwara K, Yoshioka Y, Kosaka N, Takeshita F, et al. The clinical relevance of the miR-197/*CKS1B*/*STAT3*-mediated PD-L1 network in chemoresistant non-small-cell lung cancer. *Mol Ther*. 2015;23(4):717–27.
62. Wang H, Zhang Z, Yan Z, Ma S. *CKS1B* promotes cell proliferation and invasion by activating *STAT3/PD-L1* and phosphorylation of Akt signaling in papillary thyroid carcinoma. *J Clin Lab Anal*. 2021. <https://doi.org/10.1002/jcla.23565>.
63. Salgado R, Toll A, Alameda F, Baró T, Martín-Ezquerria G, Sanmartín O, et al. *CKS1B* amplification is a frequent event in cutaneous squamous cell carcinoma with aggressive clinical behaviour. *Genes Chromosomes Cancer*. 2010;49(11):1054–61.
64. Akyurek N, Drakos E, Giaslaktiotis K, Knoblock RJ, Abruzzo LV, Ning Y, et al. Differential expression of *CKS-1B* in typical and blastoid variants of mantle cell lymphoma. *Hum Pathol*. 2010;41(10):1448–55.
65. Fonseca R, Van Wier SA, Chng WJ, Ketterling R, Lacy MQ, Dispenzieri A, et al. Prognostic value of chromosome 1q21 gain by fluorescent in situ hybridization and increase *CKS1B* expression in myeloma. *Leukemia*. 2006;20(11):2034–40.
66. Jia Y, Tian Q, Yang K, Liu Y, Liu Y. A Pan-Cancer Analysis of Clinical Prognosis and Immune Infiltration of *CKS1B* in Human Tumors. *Biomed Res Int*. 2021;2021:5862941.
67. Kamitaki N, Hujoel MLA, Mukamel RE, Gebara E, McCarroll SA, Loh PR. A sequence of SVA retrotransposon insertions in ASIP shaped human pigmentation. *Nat Genet*. 2024;56(8):1583–91.
68. Konkol MK, Walker JA, Hotard AB, Ranck MC, Fontenot CC, Storer J, et al. Sequence Analysis and Characterization of Active Human Alu Subfamilies Based on the 1000 Genomes Pilot Project. *Genome Biol Evol*. 2015;7(9):2608–2622.
69. Larsson A. AliView: a fast and lightweight alignment viewer and editor for large datasets. *Bioinformatics*. 2014;30(22):3276–8.
70. Team J. JASP (Version 0.19.0). Amsterdam: University of Amsterdam; 2024. Available from: <https://jasp-stats.org/>.
71. Benson DA, Cavanaugh M, Clark K, Karsch-Mizrachi I, Lipman DJ, Ostell J, et al. GenBank. *Nucleic Acids Res*. 2018;41:36.
72. Wolfe D, Dudek S, Ritchie MD, Pendergrass SA. Visualizing genomic information across chromosomes with PhenoGram. *BioData Min*. 2013;6(1):18.

## Publisher's Note

A list of authors and their affiliations appears at the end of the paper.